An Accelerated Explicit Method with a Two-Stage Computation Scheme for Transient Thermal Stress and Welding Deformation†

MA Ninshu*

Abstract

An accelerated explicit method with two-stage computation scheme is developed for simulating transient thermal stress and deformation occurring in a long time welding heating and cooling process. The first computation stage is based on a dynamic explicit method considering the characteristics of the welding mechanical process by controlling both the temperature increment and time scaling parameter. In the second computation stage, a static equilibrium computation scheme is implemented after dynamic thermal loading to obtain a static solution of transient thermal stress and welding deformation. In the two-stage computation scheme, a damping parameter was determined based on a transient radial eigenvalue, which corresponds to a transient welding deformation and is automatically computed using the mass center velocity of the finite element model. The validity of the accelerated explicit method is verified by comparing the transient thermal deformation and residual stresses with those computed by the implicit FEM and experimental measurements.

KEY WORDS: (Accelerated explicit method), (Two-stage computation scheme), (Transient radial eigenvalue), (stabilization computation), (Thermal stress), (Welding deformation)

1. Introduction

Since the finite element method (FEM) was established in 1950s-1960s by Argyris [1], Clough [2], Zienkiewicz [3] and other pioneers, it has been widely used in various fields. Today, two types of the finite element method, the implicit FEM [3] and the explicit FEM [4-9], are selectively employed depending on the characteristics of problems to be solved. The implicit FEM is generally used for static problems or quasi-static problems such as the static stress or the transient stress and strain induced in metal forming, welding and fatigue cycling. The explicit FEM is often applied to compute the short time dynamic response due to impact loading. To compute the quasi-static stress and strain by the dynamic explicit FEM, Liu et al. [5, 6] applied the explicit method and the implicit method to different zones in a FE model. To improve the efficiency of the dynamic explicit method for thin-walled structures, Belytschko et al. [7] developed a center integration shell element with hourglass control algorithm and Gilbertsen et al. [8] employed parallel computation. Oden [9] analyzed the static deformation by explicit time integration using a proper damping parameter. Underwood [10] proposed a dynamic relaxation method for the transient quasi-static analysis and Paradrakakis [11] developed a method to automatically evaluate the critical eigenvalue.

In the field of computational welding mechanics, Ueda [12], Hibbit [13], Goldak [14] and Karlsson [15] started their researches and applications of the finite element method in 1970s-1980s. Since Ueda and Yamakawa [12] proposed a thermal elastic-plastic material model for welding thermal stress based on the static implicit finite element method, the implicit FEM was mainly used for welding thermal-mechanics coupling simulations [16-25]. Brown and Song in 1992 [19] simulated the welding deformation and residual stresses of one meter ring structure in 1992, which was a large model at that time. Lindgren et al. in 1997 [20] reduced the computer time by applying dynamic meshing scheme to implicit FEM. In the recent decade, Murakawa et al. [21] and Nishikawa et al. [22] in 2004 reduced computation time with a fast iterative substructure method (ISM) in which the global FE model was divided into a large linear zone and a small nonlinear zone according to the transient temperature distribution during welding. Furthermore, considering a little effect the constraint located away from the welding zone on the welding induced inherent strain [17], Murakawa et al. in 2014 [23] developed the inherent strain based ISM named as i-ISM in which the nodes in the zones away from

† Received on July 11, 2015

* Guest Professor

Transactions of JWRI is published by Joining and Welding Research Institute, Osaka University, Ibaraki, Osaka 567-0047, Japan

welding line are constrained and released repeatedly at several certain steps. Huang et al. [24] modified the ISM and implemented large strain terms for the welding deformation computation in lap joints of thin plates. With the aid of the implicit FEM enhanced by ISM, Ma et al. [25] analyzed the residual stresses induced by laser –arc hybrid welded butt joints. Andersen in 2000 [26] investigated residual stresses and deformations in large ship structures using a solid element model for welded joints and a shell element model for welded structures, respectively. Deng et al. [27] focused the welding residual deformation using implicit FEM and shell element models based on inherent deformation concept. He successfully predicted welding assembly deformation using interface element which was employed to model the joining of weld lines before and after welding. Lindgren in 2006 [28] reviewed the recent development and progress of computational welding mechanics. He indicated that parallel computing used in implicit finite element methods reduced the computer time and that used in explicit finite element methods had better scalability.

Compared with the implicit FEM, the explicit FEM has a great advantage in solving large scale FE models because it uses a small amount of computer memory and its parallelized program has a good performance. Therefore, the explicit FEM has been successfully used to simulate dynamic phenomena of very large automobile structures under impact loading [29] and quasi-static mechanical phenomena in metal forming processes [30]. Because the welding heating and cooling time is long, the direct application of the standard dynamic explicit FEM with very small explicit time step may take a long computation time. Ma et al. in 1998 [31] made a first trial simulation using a dynamic explicit FEM with a mass scaling technique for the thermal buckling deformation in a butt welded joint of thin aluminum sheets. In 2008 Ma and Umezu [32] summarized the techniques of how to use commercial dynamic explicit FEM software for the simulation of the welding thermal deformation. However, the commercial dynamic explicit FEM software cannot consider the welding characteristics such as the filling of the welding groove. Recently, Shibahara et al. in 2011 [33] proposed an idealized explicit finite element method using an assumed mass matrix and a damping matrix for the simulation of the quasi-static welding thermal stress and deformation. Ikushima et al. [34] employed GPU for parallel computation and simulated welding residual stresses produced in a large scale multi-pass butt welded joint of thick plates. However, the simulation on the welding deformation especially induced in the thin-walled structures was not reported.

In the current work, an accelerated explicit method with two-stage computation scheme is developed for simulating transient thermal stress as well as deformation occurring in welding heating and cooling processes. The first computation stage is based on the dynamic explicit FEM considering the characteristics of welding mechanical processes by controlling both the temperature increment and time scaling parameter. In the second computation stage, a static equilibrium computation scheme based on a dynamic relaxation algorithm is implemented after thermal loading in order to obtain a quasi-static solution of transient thermal stress and welding deformation. In this two-stage computation scheme, a damping parameter is automatically determined using the transient radial eigenvalue computed from the velocity at the mass center of the finite element model. The validity of the developed accelerated explicit method is verified by comparing the transient thermal stress and welding deformation with those obtained by an implicit FEM [23-25] and experimental measurement.

2. Accelerated explicit method with a two stage computation scheme

2.1 Standard dynamic explicit

A general equation of motions and its transformed form are respectively given by Eq.(1) and Eq.(2).

$$Ma + Cv + Ku = F_{ext} \tag{1}$$

$$\begin{aligned} Ma(t+dt) &= F_{ext}(t+dt) - Cv(t) - Ku(t) \\ &= F_{ext}(t+dt) - F_{damp}(t) - F_{\mathrm{int}}(t) \end{aligned} \tag{2}$$

Where, M, C, K and F_{ext} are the mass matrix, damping matrix, stiffness matrix and external force. Since the second term Cv and the third term Ku represent, respectively, the damping force F_{damp} and internal residual force F_{int}.

If the above motion equation is combined with FEM, the diagonal mass matrix , the equivalent external nodal force , the equivalent internal nodal force and the damping nodal force can be computed by following equations,

$$M = \int_{Vol} \rho \{N_i N_i\}^T \cdot dVol \tag{3}$$

$$F_{ext}(t+dt) = P_{concentrae}(t+dt) + P_{pressure}(t+dt) \tag{4}$$

$$F_{\mathrm{int}}(t) = \int_{Vol} B \cdot \sigma(t) \cdot dVol \tag{5}$$

$$F_{damp}(t) = C \cdot v(t) \tag{6}$$

Where, ρ, N_i, Vol are the mass density of materials, the shape function of element and the volume of finite element model; the external nodal force $F_{ext}(t+dt)$ includes the concentrated nodal force $P_{concentrae}$, the nodal force due to external pressure $P_{pressure}$and others such as the contacting nodal force; B is a matrix describing the relation between strains at integration points and nodal displacements in an element; σ is the stress vector in elements.

To solve the motion equation (2), a very small time increment dt given by the following equation must be used according to Courant-Frederic's-Lewy Condition [35].

$$dt \le \frac{L_e}{c} \tag{7}$$

Where, the L_e in the above equation is the equivalent

length of elements and c is the propagation speed of stress wave in materials given by following equation.

$$c = \sqrt{\frac{E(1-\nu)}{(1+\nu)(1-2\nu)}\frac{1}{\rho}} \quad (8)$$

Where, E, ν are the Young's modulus and Poisson's ratio.

2.2 A two stage computation scheme for Accelerated explicit method

It is well known that the time increment *dt* used in the explicit FEM, which is calculated by Eq. (7), is the order of 10^{-7} sec for steels if the element size is about 1.0 mm. If the total time of welding heating and cooling processes is assumed to be 1000 seconds, the computation cycles of explicit FEM can be the order of more than 10^{+10} and the computation may not ended within the acceptable time. Since the time of a welding thermal process can be the order of hours, the standard explicit FEM is quite difficult to adopt to simulate the quasi-static thermal stress and welding deformation. To simulate the long time phenomena occurring in welding thermal cycles, a two-stage computation scheme using the explicit FEM on the accelerated explicit time domain and a stabilization computation for static solution, is developed as schematically shown in Fig. 1. The accelerated explicit time domain Δt^{ACEXP} is determined with consideration of the time interval Δt^{real} and temperature increment in welding thermal cycles. This simulation method is here called accelerated explicit method abbreviated to ACEXP for easy description in the following sections. If the 2nd stage stabilization computation is skipped, the method becomes an explicit method for dynamic solution under the accelerated time domain.

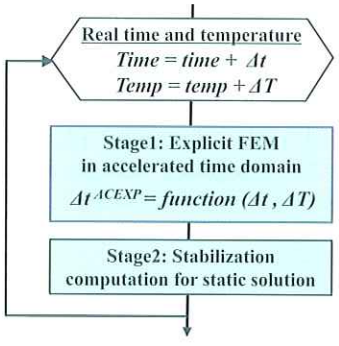

Fig. 1. A two-stage computation scheme of accelerated explicit method

2.2.1 Accelerated explicit time domain

To use the explicit method for the long time (e.g.1000sec or more) phenomena produced in a thermal loading process shown in Fig. 2, the real time has to be scaled or accelerated many times (e.g.1000 times or more) without changing the thermal loads as schematically shown in Fig. 3. For the easy understanding, the real time domain, time domains for the thermal conduction implicit FEM and for the ACEXP method are schematically represented in Fig. 4. To distinguish the very small explicit time increment determined by Eq. (7), the real time increment denoted by Δt^{real} and the time increment Δt^{therm} for thermal conduction analysis are named as the real time interval and the thermal time interval, respectively. The corresponding time interval in the accelerated explicit analysis is denoted by Δt^{ACEXP}. The similar symbols for real time, the time for thermal conduction analysis and the time for the ACEXP method are denoted by t^{real}, t^{therm}, t^{ACEXP}, respectively. In the welding thermal conduction simulation using implicit FEM, a thermal time interval Δt^{therm} is generally set to be equal to the real time interval Δt^{real}.

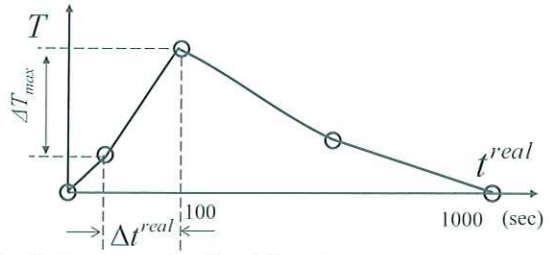

Fig. 2. An example of welding thermal cycle in the real time domain.

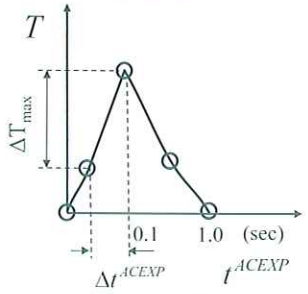

Fig. 3. An example of thermal cycle in the accelerated explicit time domain.

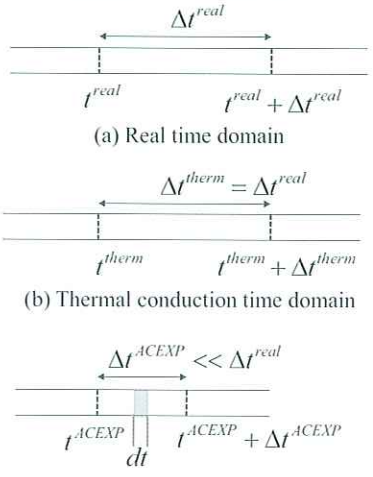

Fig. 4. Various time domains for real phenomena, thermal conduction and accelerated explicit method.

Fig. 4. Various time domains for real phenomena, thermal conduction and accelerated explicit methods.

In this developed explicit method for stress and strain simulation, the accelerated explicit time interval Δt^{ACEXP} corresponding to the real time interval Δt^{real} is set by Eq.(9) using the combination of the time based scaling parameter t_{scale} and the temperature increment dT based time converting scheme with the consideration of the characteristics of welding thermal cycles.

$$\Delta t^{ACEXP} = \frac{\Delta t^{real}}{t_{scale}} + \frac{\Delta T_{\max}}{dT} dt \tag{9}$$

Where, $\Delta T_{\max}$ is the maximum temperature change in the real time interval Δt^{real} and dt is the explicit time given by Eq.(7).

The first term in the equation (9) uses the conventional mass scaling technique [13]. The second term is based on the temperature increment control method used in the implicit FEM [17] and in an idealized explicit FEM [14]. Based on this time accelerating scheme, the explicit computation cycles or the computation time at the first stage will be controlled by the two parameters t_{scale} and dT. Their combination is better to control both the computation accuracy and computation time which is proportional to the explicit cycles.

2.2.2 Stabilization computation scheme for static solution

Usually, the dynamic explicit solution does not satisfy the static mechanical equilibrium condition. Therefore, to obtain the static solution of welding thermal stress and deformation, a stabilization computation with repeating explicit cycles at the fixed real time is performed based on a dynamic relaxation algorithm [10]. To save the computation time without losing the accuracy, the stabilization computation can selectively conducted once every certain step intervals Nc as shown in Fig. 5.

During the stabilization computation, the ratio E_{ratio} of kinematic energy to internal energy and the ratio U_{ratio} of the normalized displacement increment to the normalized total displacement of the FE model are defined by Eqs.(10-11), respectively. If the ratios E_{ratio} and U_{ratio} are less than their tolerances E_{tol} and U_{tol}, respectively, the results computed by ACEXP can be considered as a static solution.

$$E_{ratio} = \frac{\sum_{i=1}^{Nodes} \frac{1}{2} m v^2}{\sum_{ie=1}^{NE} \bar{\sigma} \cdot \bar{\varepsilon} \cdot V_e} < E_{tol} \tag{10}$$

$$U_{ratio} = \frac{\sum_{i=1}^{Nodes} \sqrt{\Delta u_x^{\,2} + \Delta u_y^{\,2} + \Delta u_z^{\,2}}}{\sum_{i=1}^{Nodes} \sqrt{u_x^{\,2} + u_y^{\,2} + u_z^{\,2}}} < U_{tol} \tag{11}$$

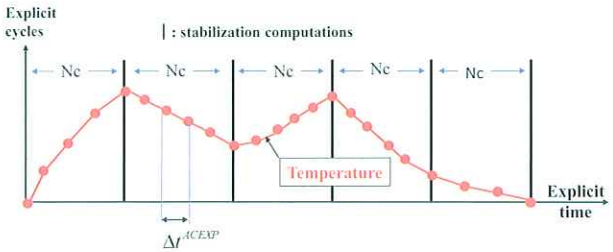

Fig. 5. Selective stabilization computation scheme at the certain thermal step intervals Nc.

The tolerances E_{tol} and U_{tol} are the order of 10^{-4} for accurate stabilization computation.

2.2.3 Estimation of transient radial eigenvalue for damping parameter

It was reported by Ma and Umezu [27] that the effect of dynamic vibrations on the welding deformation can be well controlled by applying a mass damping force given by following equation based on the minimum vibration radial eigenvalue $\omega_{\min}$.

$$F_{damp}(t) = 2.0\omega_{\min} \cdot M \cdot v(t) \tag{12}$$

To get the minimum radial eigenvalue $\omega_{\min}$ of a global FE model, generally the eigenvalue analysis based on the implicit FEM has to be performed previously. If the degrees of freedom of FE models become too large, the memory requirement and computation time will be very long. On the other hand, the minimum eigenvalue computed by the implicit FEM may not fit the transient welding deformation mode which is changing during welding and subsequent cooling processes. For these reasons, an explicit estimation method for the dynamic eigenvalue was suggested by Papadrakakis [11]. By referring to this method, a transient radial eigenvalue corresponding to the transient welding deformation mode at time $\omega_{def}(t)$ is computed by Eq. (13). The parameter $g(t)$ in Eq. (13) is computed using the integrated velocity from all nodes of a global FE model defined by Eqs. (14-15). The integrated velocity is here called the mass center velocity of the FE model.

$$\omega_{def}(t) = \frac{|1 - g(t)|}{dt \cdot \sqrt{g(t)}} \tag{13}$$

$$g(t) = \frac{v_g(t)}{v_g(t - dt)} = \frac{\sqrt{v_g^x(t)^2 + v_g^y(t)^2 + v_g^z(t)^2}}{\sqrt{v_g^x(t - dt)^2 + v_g^y(t - dt)^2 + v_g^z(t - dt)^2}} \tag{14}$$

$$v_g^x(t) = \frac{\sum_{i=1}^{Nodes} M_i v_i^x(t)}{\sum_{i=1}^{Nodes} M_i} \quad v_g^y(t) = \frac{\sum_{i=1}^{Nodes} M_i v_i^y(t)}{\sum_{i=1}^{Nodes} M_i} \quad v_g^z(t) = \frac{\sum_{i=1}^{Nodes} M_i v_i^z(t)}{\sum_{i=1}^{Nodes} M_i} \tag{15}$$

Where, $v_g(t)$ and $v_g(t - dt)$ are the mass center velocities at time (t) and at time $(t + dt)$, respectively.

Using the transient radial eigenvalue $\omega_{def}(t)$, the

damping force in the developed accelerated explicit method is given by following equation.

$$F_{damp}(t) = 2.0\omega_{def}(t) \cdot M \cdot v(t) \quad (16)$$

2.3 Stress and strain computation

When the acceleration $a(t+dt)$ at the nodes of FEM using Eq. (2) is obtained, the nodal velocity $v(t+dt)$, the nodal displacement increment $du(t+dt)$ can be easily computed in sequence by Eq. (17) and Eq. (18), respectively.

$$v(t+dt) = v(t) + a(t+dt) \cdot dt \quad (17)$$

$$du(t+dt) = v(t+dt) \cdot dt \quad (18)$$

Then, strain increment $d\varepsilon(t+dt)$ at the integration points of elements can be computed by Eq. (19).

$$d\varepsilon(t+dt) = B \cdot du(t+dt) \quad (19)$$

Where, B is the matrix describing the relationship between strain and nodal displacement in an element.

The thermal stress $\sigma(t+dt)$ can be computed based on thermal elastic plastic theory [12, 17] using the following equation.

$$\sigma(t+dt) = \sigma(t) + D(T) \cdot (d\varepsilon - d\varepsilon^T - d\varepsilon^p) \quad (20)$$

Where, the $d\varepsilon^T, d\varepsilon^p$ and $D(T)$ are the thermal strain increment, plastic strain increment and material elastic matrix, respectively. The thermal strain increment and plastic strain increment are given by Eq. (21) and Eq. (22), respectively.

$$d\varepsilon^T = \alpha(T) \cdot dT + \frac{dD(T)}{dT} D^{-1}(T) \cdot \sigma(t) \cdot dT \quad (21)$$

$$d\bar{\varepsilon}^p = \frac{\bar{\sigma}_{try}(t+dt) - \sigma_Y(T+dT, \bar{\varepsilon}^p)}{3G(T) + H'(T)}, \quad d\varepsilon_{ij}^p = d\bar{\varepsilon}^p \frac{\partial \bar{\sigma}}{\partial \sigma_{ij}} \quad (22)$$

Where, $\alpha(T)$, $G(T)$ and $H'(T)$ are the transient thermal expansion coefficient, shear modulus and plastic work hardening tangent coefficient of materials at temperature (T). σ_Y is the yield stress of materials changing with the temperature and equivalent plastic strain. $\bar{\sigma}_{try}(t+dt)$ is the elastically trial equivalent stress when a radial return algorithm is employed for the stress update.

2.4 Flow chart of accelerated explicit FEM program

Based on the proposed accelerated explicit method, a FEM program was developed. The flow chart of accelerated explicit FEM program is shown in Fig. 6. The left side of the flow chart shows the main loop in which a temperature file for welding thermal cycles is read, the accelerating time interval Δt^{ACEXP} is determined and results are written out. The right side of the flow chart expresses the computation procedures from nodal acceleration to stress update of the accelerated explicit FEM. Since the work in the right side is just simple calculations, the parallel computing using multi-cores of CPU or GPU will greatly reduce the computation time.

When the thermal cycles for all nodes were read from a temperature file which was previously computed by thermal conduction FEM and the accelerated explicit time interval Δt^{ACEXP} was set, the acceleration $a(t+dt)$ can be easily computed using Eq. (2) with a very small explicit time step dt. Then, the velocity, displacement increment, strain increment and stress are computed in sequence. When the accumulated explicit time $\sum dt$ reached the accelerated time interval Δt^{ACEXP}, the stabilization computation started. The new scheme used in this accelerated explicit method is emphasized in the flow chart by a light blue background. The computations are continued until the real time reached the end time defined in the input data.

Since this article is only focused on the development of the analyzing method for transient stress and welding deformation, the descriptions of implicit FEM for welding thermal conduction analysis are neglected. The nodal temperature and its change with time during welding and cooling processes are saved into a temperature file for stress and strain calculation using ACEXP FEM.

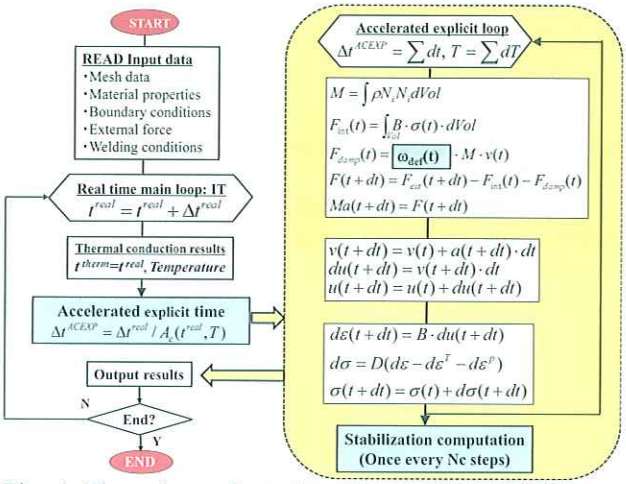

Fig. 6. Flow chart of accelerated explicit FEM program and adopted new schemes.

3. Verification of ACEXP method using a basic model

3.1 Descriptions of a basic bead welding model

To verify the accuracy of the proposed accelerated explicit method, a section model of a very long bead on plate welding plate used a welding simulation book [17] is selected as shown in Fig. 7(a). The model dimensions in the x, y and z directions are 1mm, 250mm and 15mm, respectively. Considering the symmetry of the temperature thermal stress and deformation in the width direction (y) of the weld line, a half of the transverse section is divided by solid elements. The mesh division and displacement boundary conditions are shown in Fig. 7. Only one solid element in the welding direction (x) is employed and the x-displacement Ux at all nodes is constrained to describe the plane strain state of the model. In the thermal conduction simulation, a volume heat

source with a uniform distribution in the rectangle prism (5.0×3.0×1.0mm) was assumed. The total volume heat generation rate is 450 (J/sec) and the heating time is 0.3333sec. The material physical properties, mechanical properties and their temperature dependency are shown in Table 1.

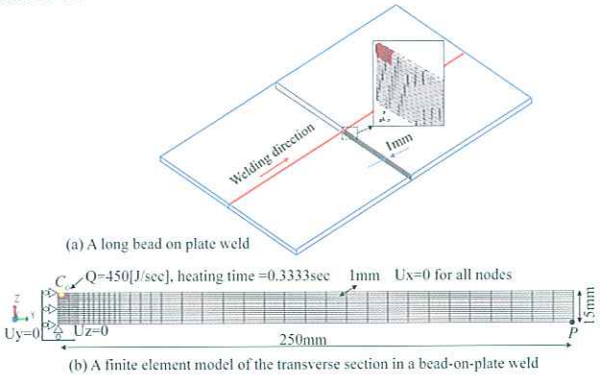

Fig. 7. A basic model of a long bead-on-plate weld.

Table 1. Temperature dependent material properties

Temperature [°C]	0.0	200.0	400.0	600.0	800.0	1000.0	1200.0
Mass density [ton/mm³]	7.82E-9	7.79E-9	7.72E-9	7.66E-9	7.61E-9	7.61E-9	7.61E-9
Specific heat [J/ton/°C]	408E+3	533E+3	658E+3	783E+3	908E+3	908E+3	908E+3
Conductivity [J/mm/s/°C]	0.05317	0.0515	0.0465	0.0382	0.0265	0.0625	0.0625
Heat transfer coef [J/mm²/s/°C]	1.0E-5	2.0E-5	4.0E-5	8.0E-5	15.0E-5	25.0E-5	25.0E-5
Thermal expansion α [1/°C]	1.0E-5	1.0E-5	1.0E-5	1.0E-5	1.0E-5	1.0E-5	1.0E-5
Young's modulus E[MPa]	2.0E+5	2.0E+5	2.0E+5	2.0E+5	2.0E+4	2.0E+4	2.0E+3
Poisson's ratio υ	0.3	0.3	0.3	0.3	0.3	0.3	0.3
Yield stress SY[MPa]	200.0	200.0	200.0	200.0	2.0	2.0	2.0
Plastic hardening Etan[MPa]	2.0E+3	2.0E+3	2.0E+3	2.0E+3	2.0E+2	2.0E+2	2.0E+2

3.2 Welding thermal cycles and temperature distribution

Fig. 8 shows the thermal cycle at the point in the welding zone computed by an implicit FEM of thermal conduction. The maximum reached temperature in the thermal cycle at the point C_o is 1576℃ which is slightly higher than the melting point of steel (1500℃). The distribution contour of the maximum reached temperature around the welding zone is also shown in the same figure. The heat affected zone (>723℃) marked by a solid line can be easily observed.

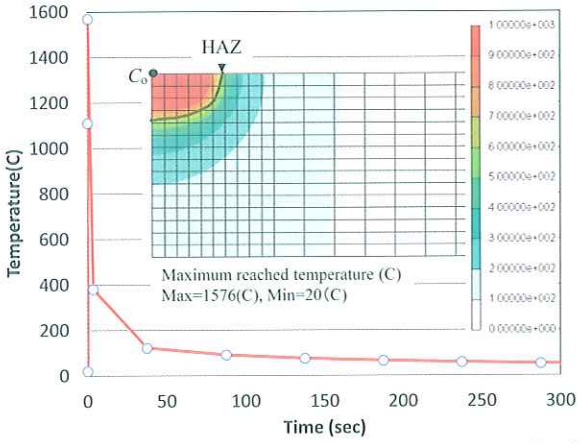

Fig. 8. Welding thermal cycle at point Co and distribution of the maximum reached temperature.

3.3 Transient radial eigenvalue

This basic bead welding model is close to a simple cantilever beam. The eigenvalue of bending deformation mode in the z direction can be easily calculated using the equation (23) based the classical elastic vibration theory [36] if the material properties (mass density scaled 1000 times, Young's modulus and Poisson's ratio) at the room temperature shown in Table 1 are used.

$$\omega_{def} = \frac{\lambda_1^2}{L^2}\sqrt{\frac{EI}{\rho \cdot Area}}$$

$$= \frac{1.875^2}{250^2}\sqrt{\frac{(2.0\times10^5)\times(15^3\cdot 1/12)}{1000\times(7.8\times10^{-9})\times(15\times1)}} \qquad (23)$$

$$\approx 39[rad/\sec]$$

The estimated transient radial eigenvalue $\omega_{def}(t)$ by Eqs. (13-15) and its change with time are shown in Fig. 9. When the time is less than about 100 sec, the temperature around the welding zone is high and the transient eigenvalue is large. When the time is longer than about 100 sec, the temperature around the welding zone becomes lower due to heat conduction and the transient radial eigenvalue saturates to a constant value. For the comparison, the constant eigenvalue computed by Eq. (23) and that computed by eigenvalue analysis using commercial FEM software LS-DYNA are also represented in the same figure. A good agreement among the computed radial eigenvalues by three methods was obtained when the temperature becomes low in the cooling process.

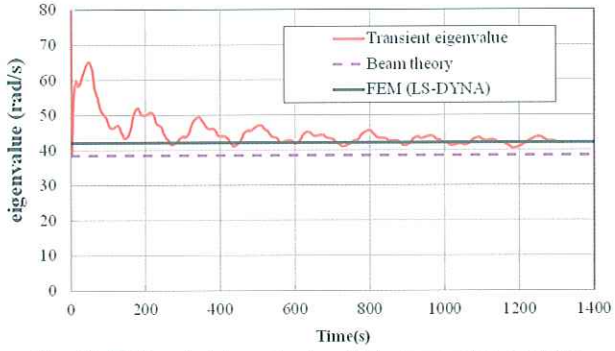

Fig. 9. Estimated transient radial eigenvalue and its change with time.

3.4 Welding deformation and thermal stresses

To verify the proposed ACEXP method, the welding induced thermal stress and deformation were computed and compared with the results by the implicit FEM. In the ACEXP computation, the time scaling factor t_{scale} and temperature increment dT used in Eq.(9) are set to be about 1000.0 and 0.1, respectively [28].

The transient deformation modes and the distribution of the z-displacement Uz(mm) during

welding and after cooling, computed by the ACEXP method, are shown in Fig. 10. The z-displacement Uz(t) at the right edge point of the model and its historical change with time are shown in Fig. 11. The welding deformation computed by the implicit FEM is also plotted in Fig. 11 and marked by cycles. It can be easily observed that the results by ACEXP method agreed very well with the implicit FEM.

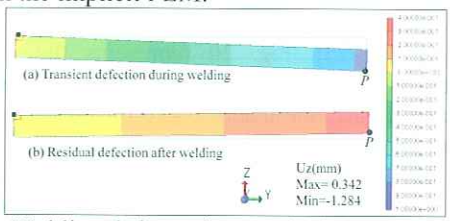

Fig. 10. Welding deformation mode during welding and cooling by ACEXP method

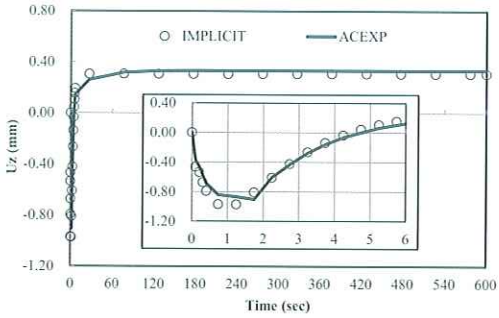

Fig. 11. History of z-displacement at edge point P during welding and subsequently cooling.

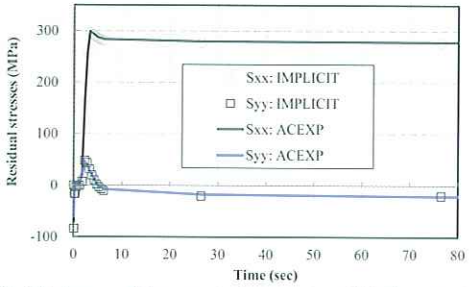

Fig. 12. History of thermal stress at welded zone during heating and cooling.

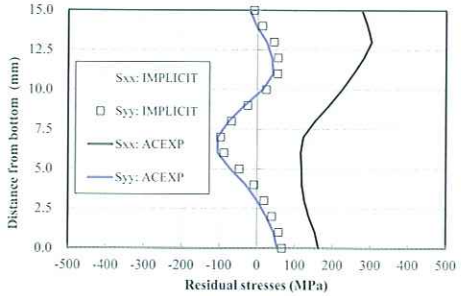

Fig. 13. Distributions of residual stresses through thickness direction.

Fig. 12 shows the historical changes of the transient thermal stresses Sxx and Syy in an element of the welded zone during heating and cooling process. The thermal stresses by the computed ACEXP method agreed very well with the results by the implicit FEM. Fig. 13 represents the distributions of stresses Sxx and Syy through the thickness direction. The residual stresses computed by ACEXP method and implicit FEM are close each other.

3.5 Effect of controlling parameters

The transient computation of the ACEXP method is controlled by three parameters which are a time scaling parameter t_{scale}, temperature increment dT defined by Eq.(9) and the stabilization computation interval . The referencing values of these parameters from the view of high accuracy are $t_{scale}=1000, dT=0.1, Nc=1$. Three additional computations were performed by changing these three parameters one by one. Fig.14 shows the transient displacement Uz(t) at the edge point P and the effect of these parameters. It can be observed that accelerating time control parameters t_{scale}, dT gave a limited influence on the transient deformation. However, the interval parameter Nc for the stabilization computation had a large effect on the transient deformation which saturated to a certain value slower than other computation cases. When $Nc=\infty$, the stabilization computation was performed only at the final step of thermal loading in order to keep the accuracy on residual results. All parameters had a little effect on the residual deformation. This means that the computed residual deformation by the proposed ACEXP method is not sensitive to input parameters.

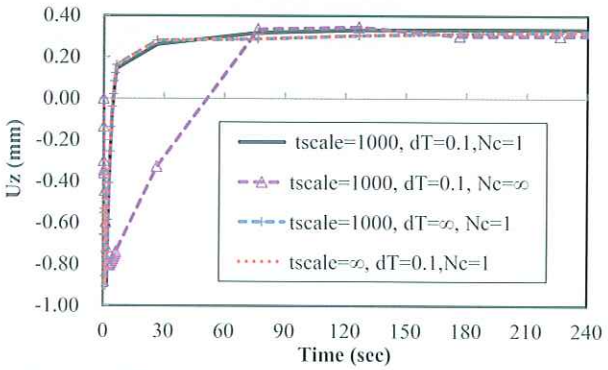

Fig. 14. Effect of controlling parameters on welding deformation.

4. Welding residual stress and deformation in a fillet joint

4.1 A fillet welding specimen and FE model

Fig. 15 shows a fillet weld in the experiment. The length, width and height of the specimen are 300mm, 200mm and 100mm, respectively. The thickness of flange and web is 4.5mm and 3.2mm, respectively. The metal active gas (MAG) arc welding process was employed in the experiment and the welding conditions are described in the figure. The base material of the plate is SS400 and the filler metal is MG-50T. As shown in Fig.15, there were six tack welds at the two sides of web plate to connect the flange and web plates before the regular one-side fillet welding. During the welding, the

fillet specimen was placed on a support plate and there was no any additional constraint.

Fig. 16 shows the mesh division with and boundary conditions of FE model. A type of eight node solid element was used. Total six nodal displacement components are constrained in order to prevent the rigid movement of the specimen. The constraints are located on the flange plate and their positions are about 30mm from the fillet weld toe. A moving volume heat source was employed in the simulation for welding thermal conduction. The welding heat source has a uniform distribution in the moving volume as shown in Fig. 16 by broken lines.

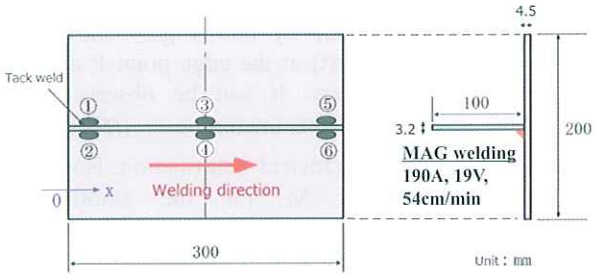

Fig. 15. A specimen of one side fillet welding.

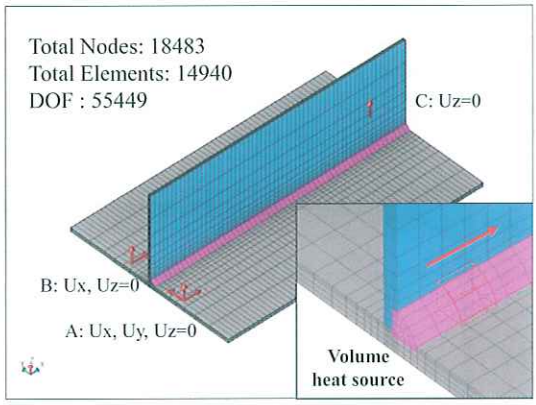

Fig. 16. FE model of fillet welded joint for simulation.

4.2 Material properties and their temperature dependence for simulation

The physical properties (mass density *den*, specific heat *c*, thermal conductivity *Lam*, heat transfer coefficient *beta* including both convection and radiation, thermal expansion coefficient *Alfa*) normalized by the values (*den0, c0, Lam0, beta0, Alfa0*) at the room temperature 20°C and their temperature dependence used in the thermal conduction simulation are shown in Fig. 17. The thermal properties of weld metal (WM) were assumed to be the same as base metal (BM). At the high temperature over 1000°C, the material properties were considered to be the same as those at 1000°C.

The mechanical properties (Young's modulus *E*, Poisson's ratio *pr*, Yield stress *SY* and linear plastic strain hardening coefficient *Etan*) normalized by the values (*E0, pr0, YS0, Etan0*) at the room temperature and their temperature dependence are shown in Fig. 18. The properties of the base metal and filler weld metal are assumed to be the same. Young's modulus, Yield stress and linear plastic strain hardening coefficient over 800°C are assumed to keep a constant value. The materials follow the isotropic linear hardening law and related plastic flow rule.

4.3 Temperature distribution

Fig. 19 shows the transient temperature distribution during welding computed by an implicit FEM of thermal conduction [23-25]. Fig. 20 represents the maximum temperature distributing on the middle transverse section. In the same figure, the macro photo of transverse section for the observation of molten zone is included. The zone where the maximum reached temperature is higher than 1400°C agreed well with the molten zone observed by macro photo. Therefore, the results of thermal conduction simulation are reliable for the subsequent simulation of thermal stress and deformation.

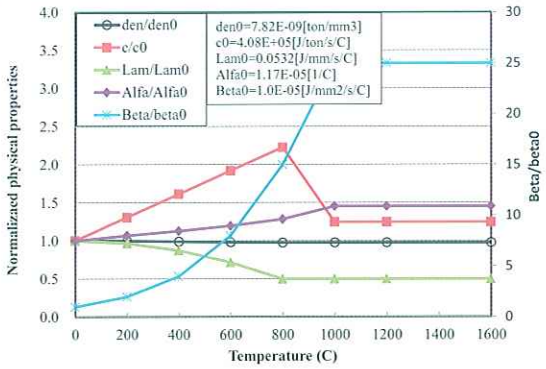

Fig. 17. Normalized thermal physical properties and their temperature dependency

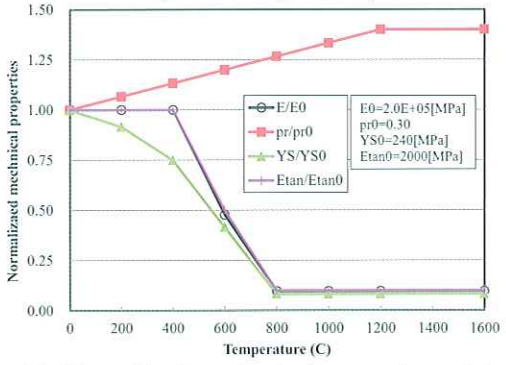

Fig. 18. Normalized mechanical properties and their temperature dependency.

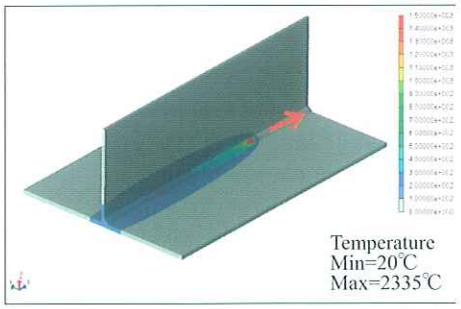

Fig. 19. Transient temperature distribution during fillet welding.

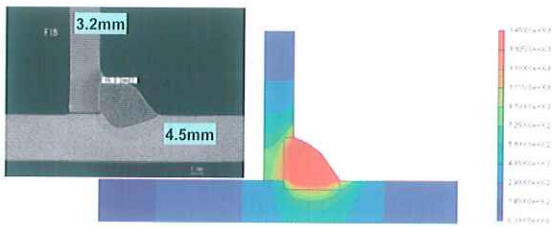

Fig. 20. The maximum temperature distribution and macro photo of transverse section.

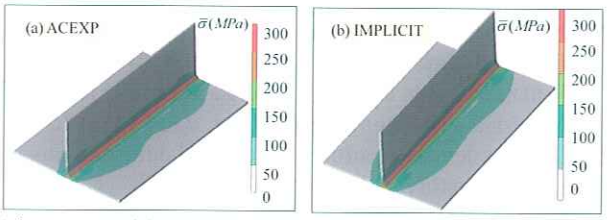

Fig. 21. Residual stress distribution computed by ACEXP FEM and implicit FEM.

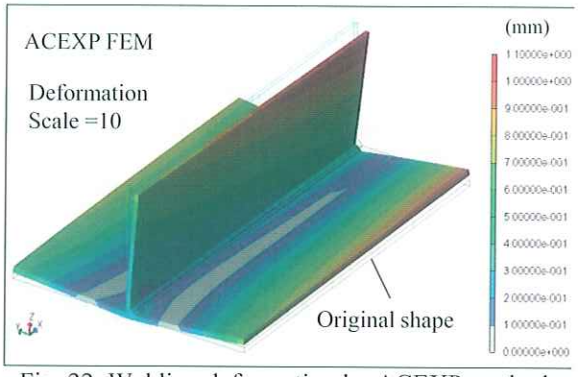

Fig. 22. Welding deformation by ACEXP method.

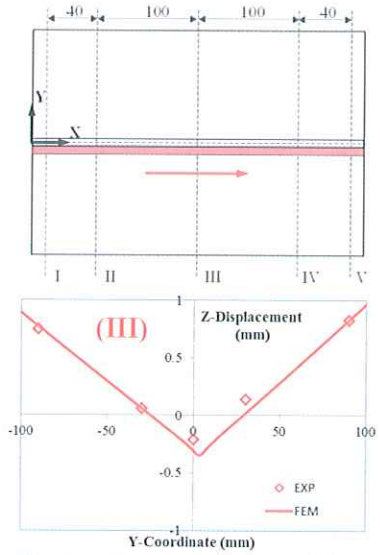

Fig. 23. The bending deformation of flange plate computed by ACEXP and comparison with experiment.

4.4 Welding deformation

Fig. 21 shows the overall deformation of the fillet weld computed by ACEXP method. Fig. 22 represents the bending deformation (z-displacement) of flange plate of the fillet joint and the comparison with measured results at the middle transverse section. A very good agreement between simulation and experiment can be observed. Therefore, the proposed ACEXP method is reliable for the prediction of welding deformation

5. Summaries

(1) An accelerated explicit method and its FEM program for the prediction of welding induced thermal stress and deformation were developed using a two-stage computation scheme, i.e., a dynamic thermal loading computation stage and a stabilization computation scheme.

(2) Transient radial eigenvalue corresponding to the transient welding deformation was automatically computed using the mass center velocity of the FE model and a damping parameter was determined.

(3) The welding deformation and residual stresses in a fillet joint of thin plates were accurately simulated using the proposed accelerated explicit method.

(4) The simulation results by the accelerated explicit method were verified through the comparison with the results by the experimental measurement and conventional implicit FEM. A good agreement was obtained, and the proposed accelerated explicit method is accurate and reliable.

References

[1] J.H. Argyris, Energy Theorems and Structural Analysis. A Generalised Discourse with Applications on Energy Principles of Structural Analysis Including the Effects of Temperature and Non-linear Stress-Strain Relations, Butterworths, London, 1960.

[2] Clough, R.W., The finite element method in plane stress analysis. Proceedings of Second ASCE Conference on Electronic Computation, Vol. 8 (1960), Pittsburg, Pennsylvania, 345–378.

[3] O.C. Zienkiewcs and Y.K. Cheung, The Finite Element Method in Conitinuous and Structural Mechanics, MCGraw Hill, 1967.

[4] J.O. Hallquist, Preliminary user's Manuals for DYNA3D and DYNAP (Nonlinear Dynamic Analysis of Solids in Three Dimension), University of California, Lawrence Livermore National Lab, Rept. UCID-17268(1976)

[5]W.K. Liu and T. Belytschko, "Mixed-Time Implicit-Explicit Finite Elements for Transient Analysis," Computers & Structure, Vol. 15 (1982), No. 4, 445-450.

[6] W. K. Liu, Y. F. Zhang, Improvement of mixed time implicit-explicit algorithms for thermal analyasis of structures, Computer Methods in Applied Mechanics and Engineering, 37(1983), 207-223.

[7] T. Belytschko, J. I. Lin, C.S. Tsay, Explicit algorithms for the nonlinear dynamics of shells, Computer Methods in Applied Mechanics and Engineering, 42 (1984) 225-251

[8] N. D. Gilbertsen and T. Belytschko, Explicit time

integration of finite element models on a vectorised, concurrent computer with shared memory, Finite Elements in Analysis and Design 7 (1990) 193-215.
[9] J.T. Oden and S.W. Key, Analysis of static nonlinear response by explicit time integration, Int. J. Numer. Meth. Engrg., 7, 225–240, 1973.
[10] P. Underwood, Dynamic relaxation, Computational Method for Transient Analysis, Edited by Belytschko and Hughes, 1 (1986), 245-263.
[11] M. Paradrakakis, A Method for the automated evaluation of the dynamic relaxation parameters, Computer Methods in Applied Mechanics and Engineering, 25 (1981), 35-48.
[12] Y. Ueda, T. Yamakawa, Analysis of thermal elastic-plastic stress and strain during welding by finite element method, Transactions of the Japan Welding Society, Vol.2 (1971), No.2, 186-196.
[13] H. D. Hibbit and P. V. Marcal, Numerical Thermo-mechanical model for the welding and subsequent loading of a fabricated structure, Computers and Structures, Vol.3 (1973), 1145-1174.
[14] J. Goldak, A. Chakravarti, M.Bibby, A new finite element method for welding heat source, J. Metallurgical and materials Transactions B, Vol.15 (1984), 299-305.
[15] M. Jonsson, L. Karlsson, L.E. Lindgren, Simulation of tack welding procedures in butt joint welding of plates, Welding Journal, 64 (1985) Issue10, 296-301.
[16] D. Radaj, Welding Residual Stresses and Distortion, Woodhead Publishing, (2003).
[17] Y. Ueda, H. Murakawa and N. Ma, Welding deformation and residual stress prevention, Elsevier, Butterworth-Heinemann (2012).
[18] P. Michaleris, Z. Feng, G. Campbell, Evaluation of 2D and 3D FEA models for predicting residual stress and distortion, ASME-Publication-PVP, 1997,347, 91-102.
[19] S. Brown, H. Song, Finite Element Simulation of Welding of Large Structures, Journal of Engineering for Industry, Transactions of the ASME, Vol. 114, Nov., 1992, 441-451.
[20] K. W. Mahin, W. Winters, T. M. Holden, R. R. Hosbons and S. R. Macewen, Prediction and Measurement of Residual Elastic Strain Distributions in Gas Tungsten Arc Welds, Welding Research Supplement, 1991, 245-260s.
[21] H. Murakawa, I. Oda, S. Itoh, H. Serizawa, M. Shibahara and H. Nishikawa, Iterative substructure method for fast FEM analysis of mechanical problems in welding, Preprints of the National Meeting of JWS, 75 (2004), 274-275.
[22] H. Nishikawa, I. Oda, M. Shibahara, H. Serizawa, H. Murakawa, Three-dimensional Thermal elastic plastic FEM Analysis for Predicting Residual Stress and Deformation Under Multi-pass Welding, Proceedings of ISOPE04 (2004), Toulon, France.
[23] H. Murakawa, N. Ma and H. Huang, Iterative substructure method employing concept of inherent strain for large scale welding problem, Welding in the World, 59-1, 2015, DOI: 10.1007/s40194-014-0178-z
[24] Hui HUANG, Ninshu MA, Tadafumi HASHIMOTO, Hidekazu MURAKAWA, Welding Deformation and Residual Stresses in Arc Welded Lap Joints by Modified Iterative Analysis, STWJ, May, 2015.
[25] N. Ma, L. Li, H. Huang, S. Chang, H. Murakawa, Residual Stresses in Laser-Arc Hybrid Welded Butt-joint with Different Energy Ratios, Journal of Materials Processing Technology, 220 (2015) 36-45.
[26] L. F. Andersen, residual stresses and deformations in steel structures, Doctor thesis, Tech. Univ. of Demark, Dec., 2000.
[27] D. Deng, H. Murakawa and W. Liang, Numerical simulation of welding distortion in large structures, Computer Methods in Applied Mechanics and Engineering, Volume 196, Issues 45–48 (2007), 4613–4627.
[28] L.E. Lindgren, Numerical modelling of welding, Comput. Methods Appl. Mech. Engrg. 195 (2006) 6710–6736.
[29] J. Hallquist, LS-DYNA user manual (1997), http://www.lstc.com/
[30] Bergman, G., and Oldenburg, M., A finite element model for thermal-mechanical analysis of sheet metal forming, Int. J. Numer. Mech. Eng. 59 (2004), 1167-1186.
[31] N. Ma, Y. Umezu and H. Murakawa, Analysis of Thermal Distortion and Residual Stresses in Welding Using LS-DYNA, Proc. 5th Int.LS-DYNA users conference (1998).
[32] N. Ma and Y. Umezu, Application of Explicit FEM to Welding Deformation, Light Metal Welding Structures,,Vol.46 (2008) No4, 142-149.
[33] M. Shibahara, K. Ikushima, S. Ito and K. Masaoka, Computational Method for Transient Welding Deformation and Stress for Large Scale Structure based on Dynamic Explicit FEM, Journal of Japan Welding Society, Vol.29 (2011) No.1, 1-9.
[34] K. Ikushima, M. Shibahara, Prediction of Residual Stresses in Multi-pass Welded Joint using Idealized Explicit FEM accelerated by GPU, Computational Material Science, Vol.93 (2014) No.7, 62-67.
[35] R. Courant, K. Friedrichs, H. Lewy, Über die partiellen Differenzengleichungen der mathematischen Physik, Mathematische Annalen, Vol.100 (1928), Issue 1, 32-74.
[36] http://www.jsme.or.jp/sed/guide/dynamics5.pdf